

## Retinal blood vessel extraction employing effective image features and combination of supervised and unsupervised machine learning methods

Mahdi Hashemzadeh<sup>a,\*</sup>, Baharak Adlpour Azar<sup>b</sup>

<sup>a</sup> Faculty of Information Technology and Computer Engineering, Azarbaijan Shahid Madani University, Tabriz-Azarshahr Road, 5375171379, Tabriz, Iran

<sup>b</sup> Department of Computer Engineering, Tabriz Branch, Azad University, Tabriz, Iran



### ARTICLE INFO

#### Keywords:

Retina  
Blood vessel  
Image processing  
Vessel extraction  
Classification  
Clustering

### ABSTRACT

In medicine, retinal vessel analysis of fundus images is a prominent task for the screening and diagnosis of various ophthalmological and cardiovascular diseases. In this research, a method is proposed for extracting the retinal blood vessels employing a set of effective image features and combination of supervised and unsupervised machine learning techniques. Further to the common features used in extracting blood vessels, three strong features having a significant influence on the accuracy of the vessel extraction are utilized. The selected combination of the different types of individually efficient features results in a rich local information with better discrimination for vessel and non-vessel pixels. The proposed method first extracts the thick and clear vessels in an unsupervised manner, and then, it extracts the thin vessels in a supervised way. The goal of the combination of the supervised and unsupervised methods is to deal with the problem of intra-class high variance of image features calculated from various vessel pixels. The proposed method is evaluated on three publicly available databases DRIVE, STARE and CHASE\_DB1. The obtained results (DRIVE: Acc = 0.9531, AUC = 0.9752; STARE: Acc = 0.9691, AUC = 0.9853; CHASE\_DB1: Acc = 0.9623, AUC = 0.9789) demonstrate the better performance of the proposed method compared to the state-of-the-art methods.

### 1. Introduction

The human eye is composed of several components: the cornea, pupil, iris, vitreous, and retina. Any abnormality in any of these can cause vision defects or even blindness. Among them, studying the retina structure and its blood vessels is very consequential [1]. An analysis of the retinal blood vessel structure provides very useful information. Ophthalmologists analyze retinal images to detect ocular and also non-ocular diseases. They can diagnose and prevent diseases such as glaucoma, hypertension, and diabetes by studying tortuosity, diameter, density, and shape of the vessels [2]. Accordingly, in order to have automatic systems for diagnosing eye diseases, various approaches in the field of retinal image processing have been proposed in recent times. Generally, the first step to design an automated system to diagnose eye diseases using retinal vascular features is the extraction of retinal vessels [3]. In fact, in such diagnosis systems, human health depends on the accuracy and reliability of this critical process. Therefore, developing a method that can extract the retinal blood vessels reliably is still an important challenge in the field of image processing and machine vision [4].

Researches in the field of retinal blood vessel extraction using image

processing are divided into two groups. The first group consists of the supervised methods like [5–19], and the second group is made up of the unsupervised methods such as [20–29]. Supervised methods are generally based on supervised machine learning algorithms, thus the rule for vessel extraction is learned by the algorithm using a training set of labeled retinal images. In contrast, unsupervised methods try to find inherent patterns of blood vessels in retinal images that can then be used to determine that a particular pixel belongs to vessel or not.

In supervised methods, a feature vector containing several components of pixels' visual features is extracted. Then, a classifier like an artificial neural network (NN) or a support vector machine (SVM) or a decision tree is trained in order to classify the image pixels into vessel and non-vessel classes based on their feature vectors. The training of the classifier is performed using a training set of retinal images with their vessel and non-vessel pixels already labeled by experts. The feature vectors used in previous studies are usually composed of the pixel intensity, two-dimensional Gabor wavelet transform taken at multiple scales, gradient vector field, morphological transformation and moment invariants-based features [30]. The performance of the supervised methods is strongly dependent on the image features that are selected for forming the feature vector.

\* Corresponding author.

E-mail addresses: [hashemzadeh@azaruniv.ac.ir](mailto:hashemzadeh@azaruniv.ac.ir) (M. Hashemzadeh), [baharak.adlpur@gmail.com](mailto:baharak.adlpur@gmail.com) (B. Adlpour Azar).

In unsupervised methods, any retinal image is processed independently. In order to increase the distinction of vessel and non-vessel pixels, usually a set of image processing operations are applied on the image. Then, a segmentation process categorizes the pixels into vessel and non-vessel segments. Mainly, in these methods thicker vessels are extracted better than the thinner ones. A complete review of the existing methods in these two groups is available in [30], where the advantages and disadvantages of the different methods are discussed.

Generally, supervised methods are more time consuming and computationally expensive than unsupervised methods due to calculation of various types of features and training of classifiers [13]. On the other hand, as supervised methods are designed based on pre-classified data, their performance is usually better than that of unsupervised ones [5,13,30]. According to the results of comparisons between different approaches performed in previous studies [13,30,31], the average accuracy of vessel detection achieved by supervised methods, in most cases, is about 1% higher than that of unsupervised methods. Considering the large number of the pixels in the retinal images, this amount of better performance equals with correct identification of a lot of pixels.

However, reliable extraction of retinal vessels still remains as a challenging task due to the presence of several issues such as the variation in vessel appearance, shape and orientations, low and uneven contrast between background and vasculature, presence of noise and abnormal regions including lesions and other pathologies [13]. Even the performance of the supervised methods fluctuates while processing various retinal images. This problem arises from the fact that there are usually considerable differences between the values of the same image features extracted from the pixels of the same class (vessel class). In different retinal images belonging to different healthy/unhealthy people, the shape, especially the thickness of vessels, and the image feature values of vessel pixels are very different because of differences in structure [15,32]. In addition, in everybody's retina, there are thick vessels that are easily visible in retinal images and thin vessels, which, in comparison with thick ones, have less clarity [30,32]. This difference in the feature values of vessel pixels in different images and the existence of thick and thin vessels in a retinal image make the values of the same features of vessel pixels to vary a lot. This may cause essential problems for training the classifiers and reduce the overall efficiency of the system. It is very difficult to provide a training set having sufficient data to cover this range of diversity. Even assuming to there is such a training set, the ability of classification algorithms to train a classifier for such data might be limited.

In this research, we propose a retinal blood vessel extraction approach utilizing effective image features and employing a combination of the supervised and unsupervised methods. Besides using the common visual features in the field of blood vessel extraction, three useful features having a significant influence on increasing the accuracy of the vessel extraction are utilized. Also, we try to take advantage of both supervised and unsupervised methods and mitigate their shortcomings, in order to propose a combined approach that extracts retinal blood vessels more accurately and reliably. The goal is to detect certain areas of vessels (thick vessels) via an unsupervised step, which performs in less time [13,30]. Then, by a supervised method having better accuracy [5,13,30], thinner vessels are extracted only from non-vessel regions detected in the previous step. This leads to the application of the classification just for the extraction of the thin retinal vessels, whose intra-class feature variance is much lower than in the case in which both thick and thin vessels are considered together. Accordingly, the remaining undetected vessel pixels can easily be distinguished from non-vessel pixels.

The proposed algorithm contains three steps: the first is the pre-processing step and it is applied in order to make the blood vessels clear in the retinal images. In the second step, based on a feature vector containing 13 features extracted from the input image, blood vessel extraction is done in two phases—clustering (unsupervised) and

classification (supervised). Ten features of this vector are common features, which are usually used in other researches of this field. Three strong features are also utilized in this research: Top Hat (TH), Shade Corrected (SC), and Bit Plane Slicing (BPS). Based on the calculated feature vector, the initial extraction of vessels is performed by using Fuzzy C-Means (FCM) clustering [33] and vessel and non-vessel clusters of pixels are acquired. The non-vessel cluster goes into a decision-tree-based classification for further processing. Other undetected vessels are also identified by this classification process. Finally, after applying a simple post-processing operation, the final blood vessels are obtained.

For evaluating the proposed method, retinal images of three publicly available databases (the DRIVE [19]<sup>1</sup>, STARE [34]<sup>2</sup> and CHASE\_DB1 [30]<sup>3</sup>) are used. Evaluation of the proposed method involves five parameters: sensitivity (Sen), specificity (Spe), positive predictive value (PPV), accuracy (Acc) and area under receiver operating characteristics (ROC) curve (AUC). The obtained results show that our approach is competitive with state-of-the-art by achieving Sen/Spe/Acc/AUC values of 0.7830/0.9800/0.9531/0.9752, 0.8087/0.9892/0.9691/0.9853 and 0.7737/0.9840/0.9623/0.9789 for the DRIVE, STARE and CHASE\_DB1, respectively. The proposed method is training set robust as it is able to provide successful vessel extraction results even when it is trained on a database and tested on another database, thus making it suitable for processing retinal images captured under different condition without retraining.

The rest of the paper is organized as follows: Section 2 provides an overview of related work. Section 3 describes the proposed method, Section 4 presents experimental results and discussions, and Section 5 draws the conclusions and ideas for future work.

## 2. Related works

The existing retinal blood vessel extraction methods can be categorized into two main groups of supervised and unsupervised methods [16,30]. Comprehensive reviews of different algorithms in these methods are available in [30]. In the following, some of the most relevant approaches from that study and the methods published later are briefly reviewed.

### 2.1. Unsupervised method

In unsupervised method, deciding about whether a pixel is a vessel or non-vessel is performed based on some similarity criteria, intrinsic features, thresholding, and some pre-specified rules on these parameters. Unsupervised methods, or in other words rule based methods, are categorized into several groups: matched filtering, morphological processes, vessel tracking, multi-scale approaches and model based algorithms. Matched filtering was used along with Laplacian of Gaussian in [25,35], and along with joint relative entropy in [24], and by using Gumbel probability distribution function in [36], and for detection of centerline and finally vessel segmentation in [37,38].

In methods proposed in [27,28] morphological operations were used along with clustering, some basic filters, classification and contourlet transform to extract the vessels. In [39] vessel tracking with local information between two points was used for vessel extraction. In some methods, multi-scale analysis based on separation of information related to the vessel width and segmentation is used for vessel extraction purpose [23,40–44]. Approaches based on vessel profile models [45], active contour models [46–48] and geometric models [26,29] which work on the basis of some models of vessel structures, are also categorized in unsupervised method group. Generally, because there is no training phase and no need for preparing labeled data, this method

<sup>1</sup> Available: <http://www.isi.uu.nl/Research/Databases/DRIVE/>

<sup>2</sup> Available: <http://cecas.clemson.edu/~ahoover/stare/>

<sup>3</sup> Available: <http://sec.kingston.ac.uk/retinal>

responds faster; on the other hand, there is the probability of not distinguishing some vessels (especially thin vessels) which can play a vital role in diagnosing various eye diseases.

## 2.2. Supervised method

Supervised machine learning method uses ground truth data (manually labeled pixels by experts) to extract the vessels and includes two steps: 1) feature extraction, and 2) classification [16]. Generally, at first, a set of labeled data is prepared for training a classifier. For each pixel in the image, some features distinguishing the vessel points from the non-vessels are extracted, and then, a classifier is trained using the extracted features. Need to labeling the data and in some cases, large dimensions of extracted features and spending relatively lots of time for training the classifiers are the disadvantages of this method. On the other side using sufficient training data and selecting an appropriate classification algorithm can result in accurate extraction of blood vessels. Method in [49] used the responses of Gaussian function and its derivatives in various scales as a feature vector and then by applying k-nearest-neighbors (KNN) algorithm expressed the probability of the pixel belonging to a vessel.

Method in [19] constructed a 27-dimensional feature vector and then used KNN classifier. Approach in [18] used a Gaussian mixture model classifier with 2-dimensional morlet wavelet. Method in [6] used a multilayer feed-forward NN as a classifier and a 7-dimensional feature vector which was composed of gray-level and moment invariants-based features to extract the retinal blood vessels. Approach in [1], by considering the main structure and the low contrast vessels discretely and applying the semi-supervised SVM classifier, separated the vessel pixels from non-vessels. Method in [17] used a feature vector including orientation analysis of gradient vector, morphological transformation, multi-scale Gabor filter and line strength features, and decision trees as the classifier. Supervised learning was performed using principal component analysis (PCA) and K-means clustering algorithm in [50]. This method applied an ensemble classification technique on the feature set analyzed by the PCA and K-means processes.

Method in [15] used a multilayer perceptron NN to determine, whether a pixel is vessel or non-vessel. Three primary color components of the retinal image were used as inputs of the NN. An improved version of the NN based classifiers was used in [14], where intensity-based and moment-invariant features were utilized to segment the retinal vessels using a lattice NN with dendritic processing. Approaches in [12,31] used Convolutional NNs (CNN) to perform the retinal vessel segmentation task. In [12], first, a multi-scale CNN architecture with an improved cross-entropy loss function was proposed to produce the probability map from image to image. Then, fully connected conditional random fields was applied to get the final binary segmentation result which made use of more spatial context information by taking into account the interactions among all of the pixels in the fundus images. In [31], a CNN was designed to extract the hierarchical features, and ensemble random forests was used as a trainable classifier.

Different from the traditional technique of supervised approach predicting the class label of each pixel in the image using image intensity or other features, method in [5] transformed the task of segmentation in a cross-modality data transformation problem. The first modality was the color retinal image and the second modality was the vessel map with the same size of input retinal image. In [51], a blood vessel segmentation and microaneurysm detection approach was proposed using discriminative dictionary learning and sparse representation. For blood vessel segmentation, two dictionaries were trained and used to classify all patches belonging to the query image. The threshold scheme was then applied to segment blood vessel patches.

Method in [13] used a 17-dimentional feature vector consists of 13 Gabor filter responses, intensity features, morphological operations, vesselness measure, and b-COSFIRE filter response. A random forest classifier was trained with the constructed feature vector in order to

detect the vessel pixels. Method in [52] first used a 30-element Gabor filter and a Gaussian fractional derivative to enhance both the blood vessel structure and its contours. Then, it applied a threshold and a series of morphology-based decision rules to isolate the blood vessels and reduce the incidence of false positive pixels.

As mentioned earlier, the main problem with the supervised methods is that there are generally considerable variations between the feature values of different pixels in the vessel class, causing the feature values of intra-class pixels to vary a great deal and influencing classification accuracy. This issue reduces the overall system efficiency.

By considering the advantages and disadvantages of the unsupervised and supervised methods, it is better to design a hybrid system that takes the advantages of both methods in order to extract the retinal vessels with the maximum possible accuracy.

## 3. Proposed method

In this section, the proposed method for retinal blood vessel extraction is presented. First the overall structure of the method is introduced. Then, the details of each step are explained in separate subsections.

### 3.1. System overview

The proposed method is designed in three steps: 1) preprocessing, 2) vessel extraction, and 3) post-processing. Fig. 1 illustrates these three steps along with the operations of each step. Each RGB retinal image that enters the system, after the application of various processing operations on it, becomes a binary image, which shows the vessel and non-vessel pixels of the input image. The preprocessing step includes the extraction of the field of view (FOV), color space transformation, the selection of suitable color channels, and contrast enhancement. The vessel extraction step includes feature extraction operations, automatic thresholding, feature vector construction, application of the PCA technique, and the extraction of the vessels using clustering and classification algorithms. The last step (i.e. the post-processing) includes a simple masking operation and the demonstration of the final extracted vessels.

### 3.2. Preprocessing

In the preprocessing step, with the purpose of enhancing the image quality and also making the subsequent operations simple and effective, the input image is gone under some operations. First, cropping the extra parts of the retinal image is performed so that only the FOV is remained. By performing this step, the next operations are executed on fewer pixels, reducing the computational complexity. Similar to the method presented in [50], the process of image cropping is performed using the FOV masks prepared for each retinal image database (see Section 4.1 for more details). First, the four extreme coordinates of FOV of each image are found using the corresponding mask. Then, the attained coordinates are used to crop the image to desired width and height. An example of cropped image is shown in Fig. 2.

Afterwards, the cropped RGB image is transformed into two L\*a\*b and YCbCr color spaces; and from any of the three color spaces the most suitable channel, namely G, L and Y, is selected. Selection of the color spaces and the channels are performed based on the very good results obtained using them in previous researches [25,50,53]. The clarity and discriminability of the vessels in these channels is high. Fig. 3 shows the examples of these three channels.

Then, the contrast limited adaptive histogram equalization (CLAHE) [54,55] is applied on the selected channels to enhance the contrast of the images and make the blood vessels clearer. The CLAHE method operates on small image regions called tiles instead of the whole image. The MATLAB implementation of this algorithm is applied to perform this operation. The required parameters in this procedure are set as

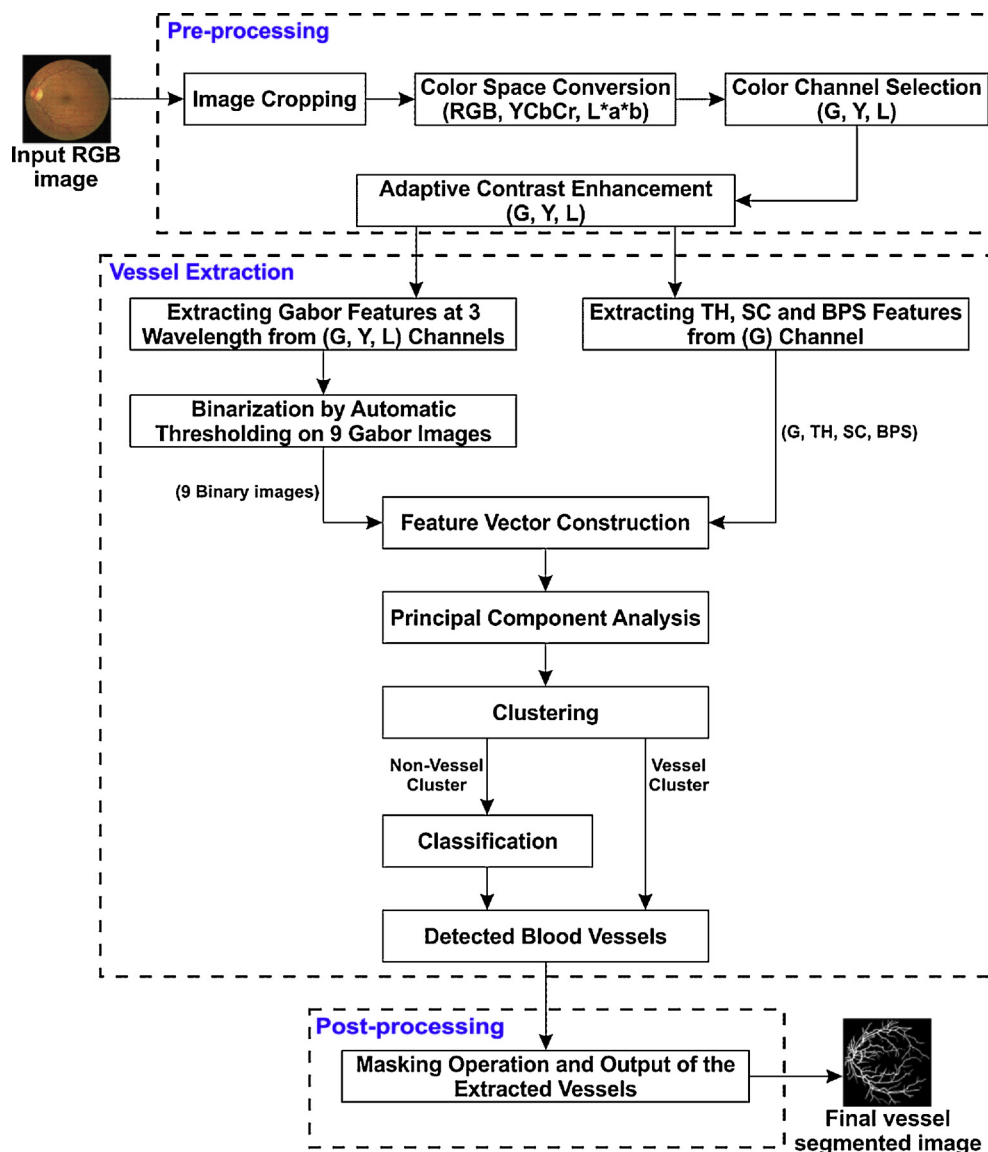


Fig. 1. Diagram of the proposed method.

follows. The size of tiles is set to  $8 \times 8$ ; the limitation of contrast enhancement is set to 0.01; the number of bins used for the histogram is 256, and the histogram shape used for the image tiles is “uniform”. The outputs of this operation on the three channels are shown in Fig. 4.

### 3.3. Vessel extraction

In the vessel extraction phase, firstly, a set of image features are extracted from three color channels and a feature vector is constructed for each pixel. Then, the constructed vector is used to separate the vessel pixels from non-vessels. Pixel separation is performed in the two steps of clustering and classification. In the following, the details of

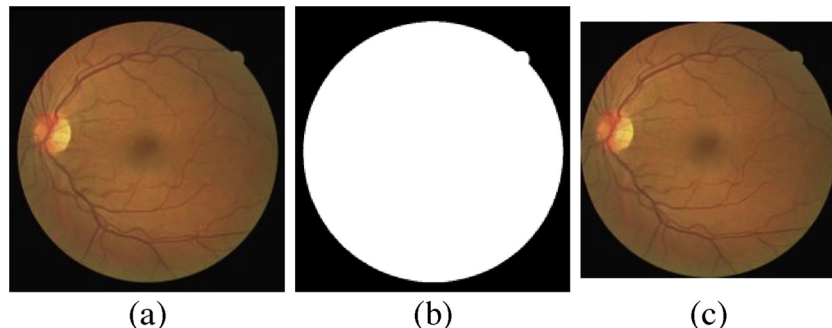
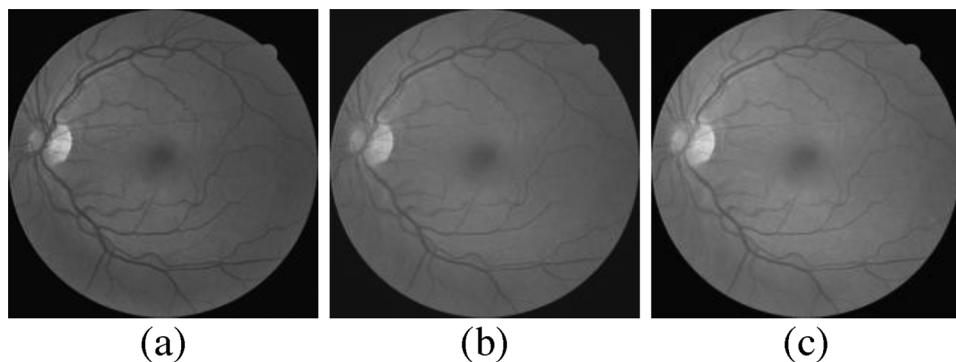
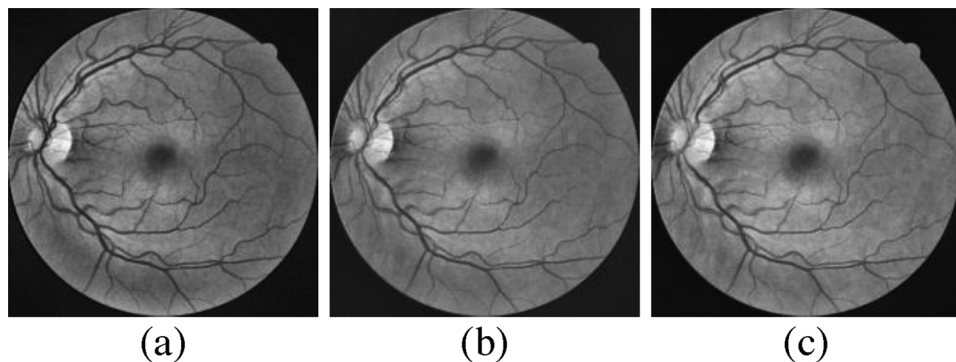


Fig. 2. (a) A sample image from DRIVE database, (b) the corresponding mask, and (c) the cropped image.



**Fig. 3.** Selected three channels. (a) G channel, (b) Y channel, and (c) L channel.



**Fig. 4.** Outputs of the histogram equalization operation on (a) G, (b) Y, and (c) L channels.

each operation in this phase are explained.

### 3.3.1. Feature extraction and feature vector construction

In the proposed method, 13 features are extracted in order to construct the feature vector for each of the image pixels. Nine features of this feature vector are obtained by applying the Gabor filter [56] on selected color channels. The tenth feature is the G channel of the RGB color space after histogram equalization. These ten features are commonly used in other researches in the field of retinal vessel extraction [3,25,45,57–60]. In the proposed method, three efficient features are also extracted by applying some basic image processing and morphological operations on the selected G channel of the RGB space. The extraction process of these 13 features is explained below.

**3.3.1.1. Gabor features.** Two-dimensional Gabor filters [56] are utilized to enhance the retinal blood vessels. These filters are sinusoidally modulated Gaussian functions which can aid in distinguishing the blood vessels [50]. Inspired by the technique applied in [25], in order to scan whole the image in all orientations and extract all the vessels in it as much as possible, multi-scale Gabor filtering is applied on each of the three images obtained from the preprocessing step. The performance of this filter is considerably influenced by the values of its parameters. Selecting the suitable parameter values leads to better performance of it. The parameters are: wavelength, aspect ratio and bandwidth that have impressive effect on Gabor kernel constructing. The size of the kernel should be in such a way to encompass all the available vessels with various width. In the proposed method, the Gabor filtering performance in vessel information extracting is in the best manner at wavelength of 9, 10, 11, aspect ratio of 0.5, and bandwidth of 1. Also, the orientation operation starts from 0 and occurs at every 15 angle. By setting the wavelength to 11 some of the thin vessels do not appear and by setting it to 9 and 10 some vessel like structures also appear. Therefore, three values are chosen for wavelength and a bank of 72 Gabor filter is created. Selecting the values of the mentioned

parameters is exactly based upon the research presented in [50].

Regarding that the filter is created in 3 scales and 3 channels are taken from 3 different color spaces, 9 images are produced in this step, i.e. three images per channel. The outputs of Gabor filters on three selected channels are shown in Fig. 5. Subsequently, a thresholding is applied to convert the obtained images into binary images representing the vessel and non-vessel pixels distinguishable at this step.

To perform the binarization operation, we design an automatic thresholding algorithm. To this end, first the Laplace filter [61] is applied on the output images of the Gabor filters. Then, each obtained image is added to its own Gabor filter image and the thresholding operation is performed on the resultant image. In this research, inspired by the thresholding method introduced in [62], a suitable and fast thresholding method is designed. The function of this method is as follows. The range of pixel values in an image is between 0 and 255. This method first counts the number of pixels having the same value of any of the values in this range. More formally,  $Y_0, Y_1, \dots, Y_{255}$  is calculated that  $Y_i$  represents the number of pixels in the image with  $i$  grey level. Then, the ratio of repetition of each one to the total image size is calculated. In other words,  $\frac{Y_0}{m \times n}, \frac{Y_1}{m \times n}, \dots, \frac{Y_{255}}{m \times n}$  are calculated that  $m \times n$  is the image size. In the next step, multiplication of each pixel by the number of its repetition is calculated and the sum of these multiplications is computed. The resulting number is the suitable threshold value for the image being processed. From the conducted experiments on various retinal images, it was figured out that by this method, the proper threshold value for different images are obtained. Fig. 6 shows the output of thresholding operation on 9 Gabor images.

**3.3.1.2. Image processing and morphological operation based features.** The features, TH, SC and BPS which are used in the proposed method, are introduced in the following. All of these three features are extracted from enhanced G channel obtained from preprocessing step.

**3.3.1.2.1. TH feature.** This feature which is extracted by using some morphological operations, is used here by the inspiration of the

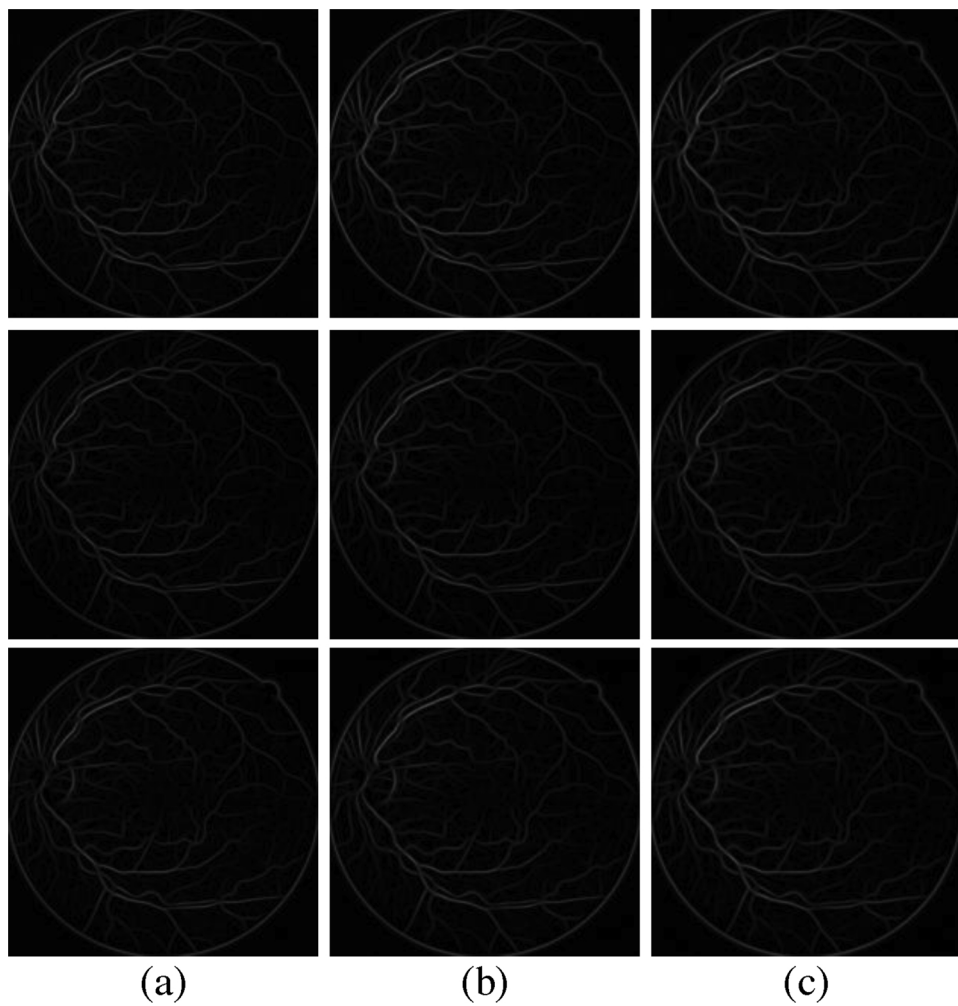


**Fig. 5.** Outputs of the Gabor filters on (first row) G, (second row) Y, and (third row) L channels with wavelength of (a) 9, (b) 10, and (c) 11.

research performed in [27]. Top Hat transformation is obtained by applying the opening morphology operation on the image and then subtracting the result image from the original image. The Top Hat transformation of image A using structure element B is expressed as Eq. (1).

$$\text{TopHat}(A) = A - (A \otimes B) \quad (1)$$

where the  $\otimes$  indicates the opening morphology operation. Selecting a proper structure element plays a vital role in the performance of this transformation. Due to the line like structures of the vessels, the linear structure element is used. In addition to the type of this element, its size is very important as well. Applying the opening operation with a structure element wider than the vessel width causes the whole vessel or some part of it to be removed. Also, if the vessel and the structure element are at the same directions, there will be no change after performing the operation. Hence, here we use the maximum result of the structure element in different directions. The length of the structure element used here is 21 pixels and its rotation is in 9 directions; starting at zero and proceeding at an interval of 22.5 angles. This transformation is applied on inverted G channel of RGB color space. This transformation has a good performance on making the vessels much clear. The result of applying this operation on a sample image is shown in Fig. 7.

**3.3.1.2.2. SC feature.** Generally, in most of the retinal images, there are light intensity variations in the background of the images that usually disrupt the system performance. By extracting the SC feature, we try to eliminate the effects of these kinds of light intensity variations

and provide a clear image [63]. The process is as follows. First, the background of the image is estimated and then subtracted from the original image. Background estimation is performed via a median filter. The median filter scans the image and selects the median of the neighboring values for each pixel. Initially, it sorts the value of the neighboring pixels and then chooses the median value. This causes the background to be uniform and the existing noises are reduced. In this step, a  $25 \times 25$  window is selected for neighboring. The output of the operations performed to extract the SC feature is shown in Fig. 8.

**3.3.1.2.3. BPS feature.** Inspired by the research performed in [38], the thirteenth feature, namely BPS feature, is utilized in the proposed method. This feature is defined as follows. Each image pixel can be represented in the form of an 8-bit array. Therefore, each image consists of eight 1-bit planes. The least significant bit planes contain details of the image and they often appear as noise, but the most significant bit planes, usually four top bit planes, contain the most of the visually important data of the image. By analyzing the resulting bit planes on various test images, it turns out that the last two planes provide better informative images. Hence, the sum of these two binary images (planes) is chosen as the BPS feature. Actually, this image contains the orientation map and the shape of the blood vessels. The output of this bit slicing task is shown in Fig. 9.

All of the thirteen features extracted for each pixel of the input image are used to construct the feature vector of each pixel which is used in subsequent processes.

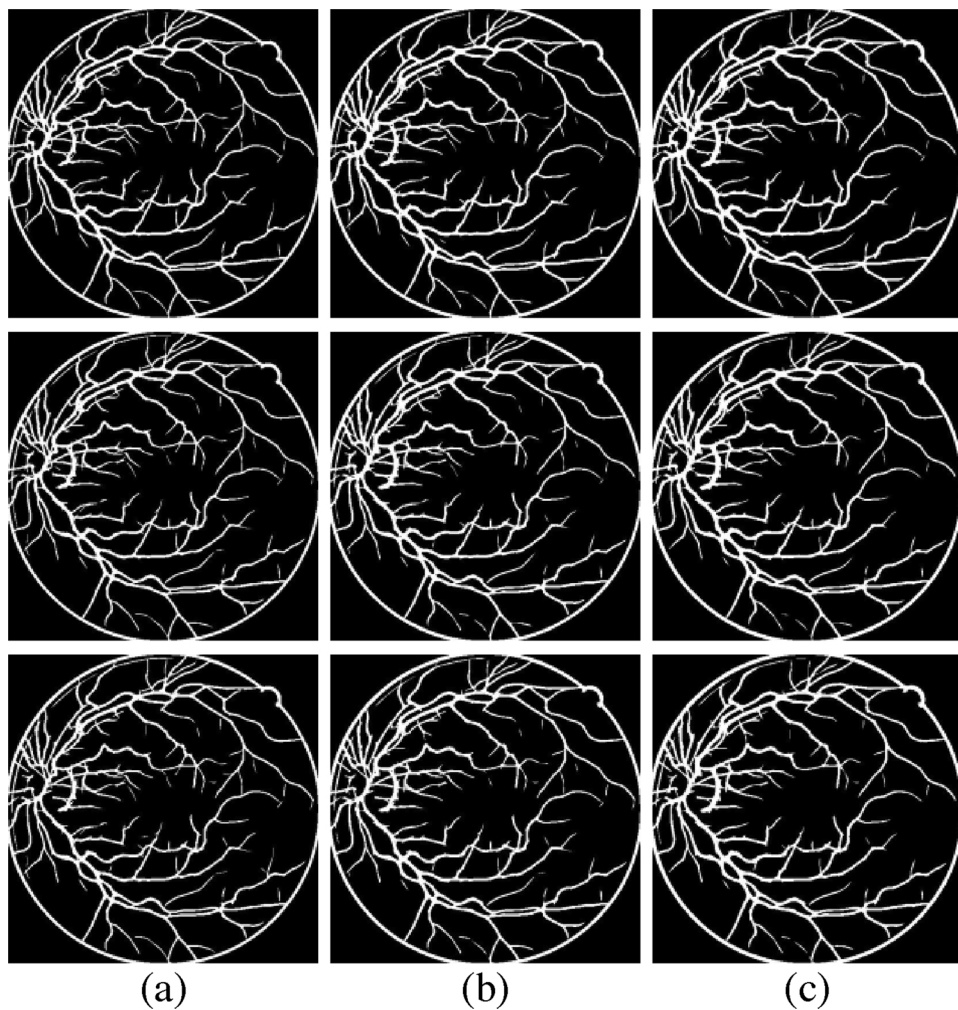


**Fig. 6.** Results of the automatic thresholding method on outputs of the Gabor filters on (first row) G, (second row) Y, and (third row) L channels with wavelength of (a) 9, (b) 10, and (c) 11.

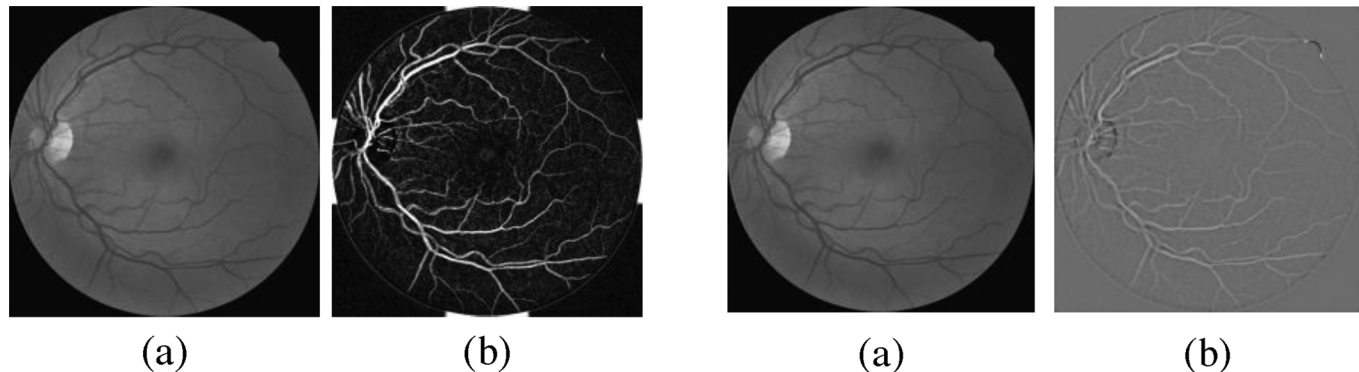


**Fig. 7.** A sample of TH feature. (a) Input image, and (b) extracted TH feature.

### 3.3.2. Principle component analysis

The 13-dimentional feature vector of the pixels enter into the PCA. The PCA technique usually plays a vital role in analyzing the multivariate data. One of the objectives of the PCA is to reduce the feature redundancy. However, in the proposed method, none of the feature dimensions are omitted. But the features are mapped into a new linear space to eliminate the correlations, if there is, between the features. After entering the feature vectors into the PCA, first, the central point is calculated; actually, the mean value is calculated in all the directions to get the new coordinates for new space. Then, subtraction of each data

from the mean value is computed, because it is assumed that the mean data for each feature is zero. And the new coordinate is obtained in this way. Subsequently, the direction in which the data variance is maximum, is obtained. Afterwards, by decomposition of covariance matrix into the eigen-vectors, it becomes diagonal. Making this matrix diagonal eliminates the correlation between the features. Finally, this vector is multiplied by the original data and the non-correlated feature vector is generated. As a result, there will be more suitable features to enter a classification or a clustering algorithm [64,65].

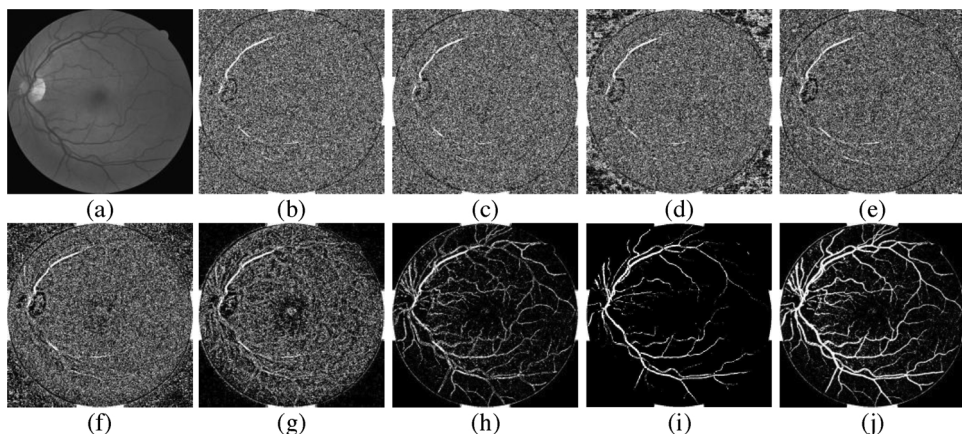


**Fig. 9.** A sample of BPS feature. (a) Input image, (b) 1st bit plane, (c) 2nd bit plane, (d) 3rd bit plane, (e) 4th bit plane, (f) 5th bit plane, (g) 6th bit plane, (h) 7th bit plane, (i) 8th bit plane, and (j) the sum of the last two bit planes.

### 3.3.3. Unsupervised vessel extraction: FCM clustering

After applying the PCA, the resulting feature vectors are used to extract the retinal vessels. To extract the thicker vessels and the vessels which have more clarity, first, an image segmentation step is performed by applying a clustering process. To this end, FCM clustering algorithm [33] is utilized. Because this algorithm uses fuzzy logic, it has a high sensitivity that leads to more accurate detection of the vessels. By applying the FCM on a dataset, each data point is assigned to a cluster to some degree that is specified by a membership grade. The fuzziness of the clusters is determined by a weighting exponent parameter  $m \in [1, \infty]$ . We use the MATLAB toolbox for performing the clustering procedure and set the required parameters as follows. The value of parameter  $m$  is set to 2, maximum number of iterations is set to 2000 as a stopping criterion, and the minimum amount of improvement being 0.000001.

This FCM clustering is applied on the obtained feature vector of image pixels to receive the membership values on each cluster for every vector. From the obtained membership values, two clusters of “vessel” and “non-vessel” pixels are determined based on the highest membership value received for each vector. Accordingly, the input retinal image is converted to a binary image. An example output of the clustering step is illustrated in Fig. 10. The size of the clusters is different; one of the clusters has more pixels in it and one of them has less. This is because most pixels of the retinal image are related to the background. Therefore, the cluster with fewer pixels is the vessel cluster and the processing on these pixels is completed in this step. For final vessel extraction (possible vessels which are not detected in this step), the other cluster goes to the next step.

### 3.3.4. Supervised vessel extraction: decision tree classification

There may be some vessel pixels which are wrongly identified as non-vessels in the previous step. Therefore, after performing the clustering step, we try to extract the thin and non-clear vessels using a supervised classification process. The classification is performed on the pixels of non-vessel cluster resulting from the clustering step. An improved version of decision tree classification algorithm, namely the root guided decision tree [66] is utilized in this step. The implementation of this classifier is performed as same as the implementation done in [50] (see [50] for more details). This classification algorithm is able to work using small amount of training data.

The classification process derives decision rules from the training data. The extracted rules can be used to classify the pixels into two classes of “vessel” and “non-vessel” pixels. The outcome of the classification procedure is a vessel probability map which consists of a value for each input pixel that determines the confidence measure of each pixel to be a vessel pixel or not. A thresholding procedure on the probability map is performed to obtain a binary image representing the vessel pixels detected in the classification step. The extracted vessel pixels in this step are combined with the vessel cluster of the clustering step to specify all the extracted vessels. Fig. 11 shows the outputs of the clustering and classification steps on an example image. As shown in this figure, most of the undetected vessel pixels in clustering step are extracted by the classification procedure.

### 3.4. Post-processing

On examining the output images of the vessel extraction phase, we observe that the border of the FOV is also recognized as vessel (as a circle or arc like structures) in a few images. In order to eliminate them, a post-processing operation is performed. To this end, the radius of the original FOV mask is reduced by some pixels such that the border of FOV not to be covered. The new mask is applied on the output image to remove those unwanted pixels. Fig. 12 shows a sample output of this step. The obtained image is the final result of the proposed method representing the whole extracted vessels.

## 4. Experiments

In this section, the overall performance of the proposed system and also the influence of each applied solution in this research are evaluated. Moreover, the results of the proposed method are compared with a series of state-of-the-art methods including traditional methods and recent approaches presented in the literature. The proposed system is implemented using the MATLAB software and a computer with a 2.50 GHz, 5 core CPU and 4 GB RAM is used to perform the experiments.

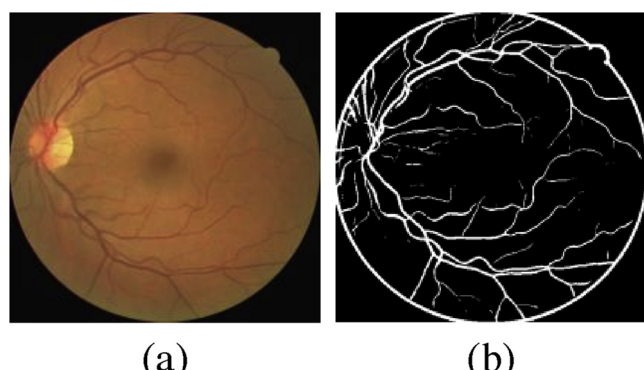


**Fig. 10.** An example output of the clustering step. (a) Input image, and (b) initial extraction of the vessels by clustering.

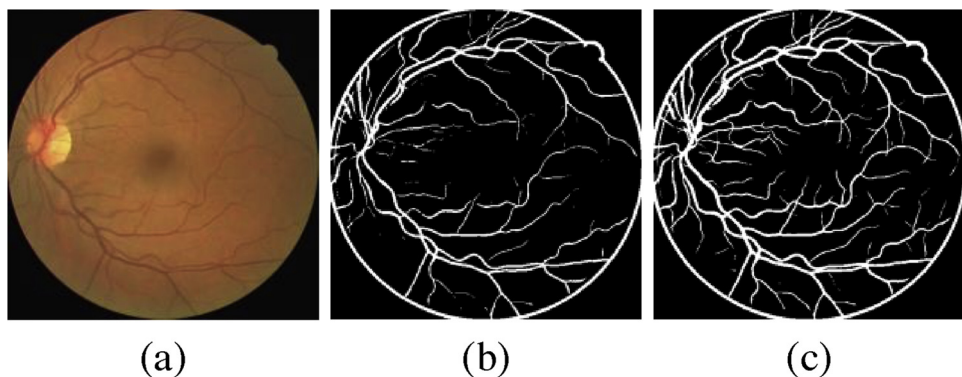


**Fig. 11.** Outputs of the clustering and classification steps. (a) Input image, (b) clustering output, (c) all extracted vessels by clustering and classification.

#### 4.1. Datasets

The performance of the proposed method are evaluated using three standard databases (the DRIVE [19], STARE [34] and CHASE\_DB1 [30]). The DRIVE database contains 40 retinal images with the size of  $565 \times 584$  pixels. These images are taken by a Canon 3CCD camera with a  $45^\circ$  field of view. Each of the images is saved by 8 bits for each channel of the RGB color space. The database has been categorized into two sets of training and test images. Each set contains 20 images. The ground truth vessels of each image is also available that can be used to evaluate the results of retinal vessel extraction methods. The performance of the proposed method is measured on the test set. In order to have a fair comparison, the training of the classifier in our approach is performed using the training set provided in a similar way to the method presented in [17]. The training is done using some samples randomly selected from each image in the training set of the database ( $2 \times 10^4$  samples such that 10,000 pixels which are selected from each image at random.)

The STARE database includes 20 retinal images with the size of  $700 \times 605$  pixels. There is no separate training and testing set available for this database. For this database, the training set is also provided in a similar way to the method presented in [17]. About 150,000 manually segmented pixels randomly selected from the 20 images (7500 pixels from each image) are used for training purpose. The testing is performed on the whole set of 20 images.

The CHASE\_DB1 database consists of 28 retinal images with a resolution of  $999 \times 960$  pixels, acquired from both the left and right eyes of 14 multiethnic school children. Most of the images in this database have non-uniform background illumination and poor contrast of blood vessels compared to the background [30] which make the vessel segmentation more difficult. Again, similar to the experiments conducted in [17], we use eight images of this database for training purpose. We select  $2 \times 10^5$  samples such that 25,000 pixels are randomly chosen from each of the images. The remaining 20 images are used for testing the

method.

For each of the three databases, two groups of manually segmented and labeled images prepared by two different observers are available. The performance of the proposed method on each database is measured by comparing the automatically extracted binary images (extracted vessels) with ones that are manually labeled by the first observer as ground truth. For DRIVE database, a binary mask for the FOV for each image is available. For STARE and CHASE\_DB1 databases, we create the FOV binary masks as described in [17,18]. Example images of three databases are shown in Fig. 13.

#### 4.2. Evaluation metrics

After getting the output of each test image, the resulting binary image is compared with its ground truth image. For each pixel, four detection cases can occur: true positive (TP), true negative (TN), false positive (FP), and false negative (FN). These four conditions are described as follows: one vessel pixel detection is TP if it is correctly identified as vessel; it is TN if correctly identified as non-vessel; one pixel is FP if it is non-vessel but is identified as vessel, and a pixel is FN if it is a vessel pixel but wrongly identified as a non-vessel one. The summations of each four detection conditions are used to get the criteria of evaluating the performance of the system on an image. The evaluation metrics are calculated only for pixels inside the FOV over all test images.

One of the criteria is accuracy. This criterion is calculated as Eq. (2).

$$Acc = \frac{TP + TN}{TP + FP + FN + TN} \quad (2)$$

The second criterion is sensitivity. This criterion shows the capability of the vessel extraction method in vessel pixel detection. This criterion is calculated as Eq. (3).

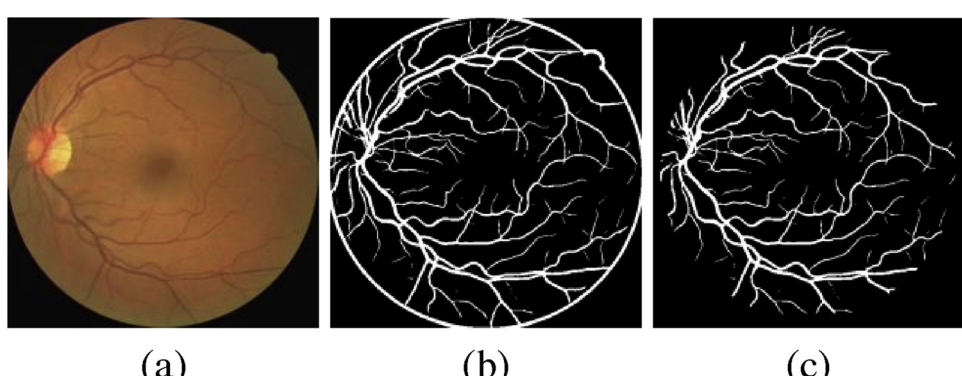


**Fig. 12.** Output of the post-processing step. (a) Input image, (b) output of the vessel extraction step, and (c) final extracted vessels after post-processing.

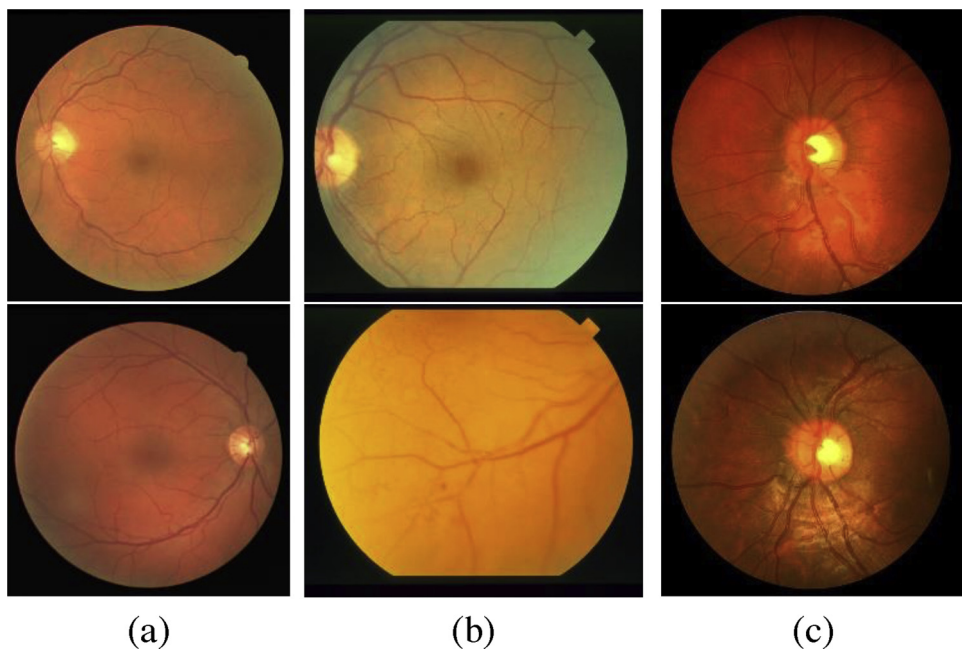


**Fig. 13.** Example images from (a) DRIVE, (b) STARE, and (c) CHASE\_DB1 databases.

$$Sen = \frac{TP}{TP + FN} \quad (3)$$

The third criterion is specificity which shows the capability of the vessel extraction method in background detection i.e. the non-vessel pixels. This criterion is computed as Eq. (4).

$$Spe = \frac{TN}{TN + FP} \quad (4)$$

The fourth criterion is the positive predictive value (PPV). It shows the number of true identifications. It is calculated as Eq. (5).

$$PPV = \frac{TP}{TP + FP} \quad (5)$$

In addition, the performance of the method is measured with the area under the received operating characteristic (ROC) curve (AUC). Because the quantitative metrics are dependent on the threshold on the probability map (constructed by the outcomes of the classification and clustering steps), an ROC curve is plotted with the true positive rate (Sen) versus false positive rate (1-Spe) by varying the threshold. The obtained ROC curve for each database is used to measure the AUC criterion. The optimal threshold values for DRIVE, STARE and CHASE\_DB1 databases are 0.57, 0.51 and 0.53, respectively.

#### 4.3. Experiment 1: results of the proposed method

After obtaining the binary vessel segmentation images in each database, the evaluation metrics are calculated. **Table 1** lists the average

**Table 1**  
Performance measures for DRIVE, STARE and CHASE\_DB1 databases.

| Database  | Method                         | Sen    | Spe    | PPV    | ACC    | AUC    |
|-----------|--------------------------------|--------|--------|--------|--------|--------|
| DRIVE     | 2 <sup>nd</sup> Human observer | 0.7796 | 0.9717 | 0.8072 | 0.9464 | –      |
|           | Proposed method                | 0.7830 | 0.9800 | 0.8594 | 0.9531 | 0.9752 |
| STARE     | 2 <sup>nd</sup> Human observer | 0.8955 | 0.9382 | 0.6432 | 0.9347 | –      |
|           | Proposed method                | 0.8087 | 0.9892 | 0.9012 | 0.9691 | 0.9853 |
| CHASE_DB1 | 2 <sup>nd</sup> Human observer | 0.8092 | 0.9699 | 0.7492 | 0.9538 | –      |
|           | Proposed method                | 0.7737 | 0.9840 | 0.8488 | 0.9623 | 0.9789 |

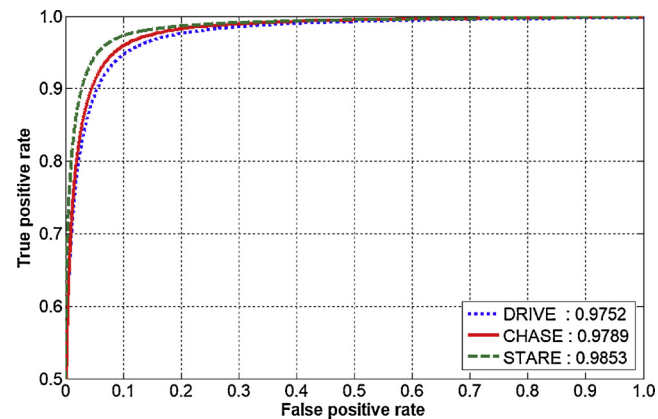


**Fig. 14.** ROC curves for DRIVE, STARE and CHASE\_DB1 databases.

performance measures calculated on all test images of each database for a comparison with those of the second human observer. The average values of Spe, PPV, Acc rates produced by the proposed method are higher than the second human observer for all three databases. **Fig. 14** shows the ROC curves obtained for each database. As illustrated in this figure, the values of AUC for the DRIVE, STARE and CHASE\_DB1 databases are 0.9752, 0.9853 and 0.9789, respectively.

The vessel extracted images with best case and worst case accuracies from the DRIVE, STARE and CHASE\_DB1 databases are shown in **Figs. 15–17**, respectively. As shown in these figures and from the results in **Table 1**, it is evident that the proposed method has accurately detected and segmented the presence of blood vessels found in retinal images of all three databases.

#### 4.4. Experiment 2: cross-training results

To measure the robustness of the proposed method against the training set, cross-training technique is applied. To this end, the classifier is trained on one of the databases and tested on another one and vice versa. This is an important experiment to evaluate the suitability of the method to be applied to any retinal image in realistic applications. The results of this experiment is summarized in **Table 2**. As shown in

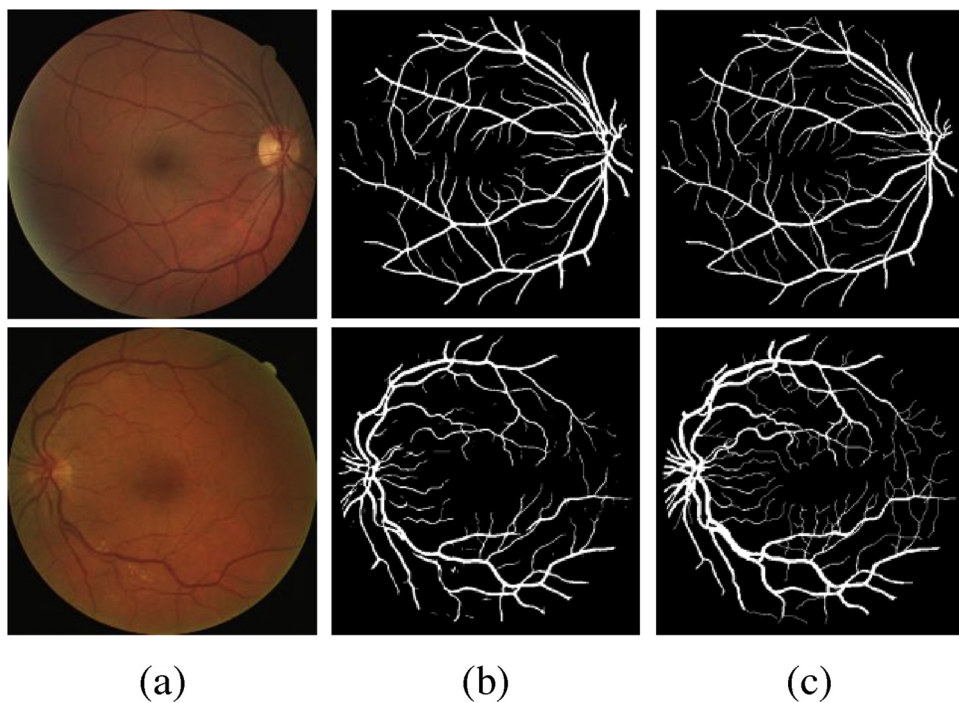


**Fig. 15.** Vessel extraction results for DRIVE database. (first row) the best case accuracy; (second row) the worst case accuracy. (a) Input image, (b) vessel extraction by proposed method, and (c) 1st Human observer.

this table, there is a slight decrease in performance as the Acc rates are decreased from 0.9531, 0.9691 and 0.9623 to 0.9499, 0.9602 and 0.9564 for the DRIVE, STARE and CHASE\_DB1 databases when they are trained on the STARE, CHASE\_DB1 and DRIVE databases, respectively. The average decrease value of Acc for all cross-training cases is 0.0058. This amount of performance drop is completely reasonable and is very close to that reported in [17]. The successful results obtained in this experiment demonstrate the robustness of the proposed method to the training set.

#### 4.5. Experiment 3: influence of the features

One of the important issues in the field of machine vision researches is extraction and selection of suitable image features. In this research, besides using the common features in the field of blood vessel extraction, three features, namely TH, SC and BPS features, are utilized to detect the vessels as well as possible. In order to analyze the effectiveness of these features on the performance of the proposed method, the implemented method is once executed with using these features and once without them on all three databases. The average results on the whole testing images of each database are illustrated in Fig. 18. As it is evident in this figure, utilization of these three features has a great

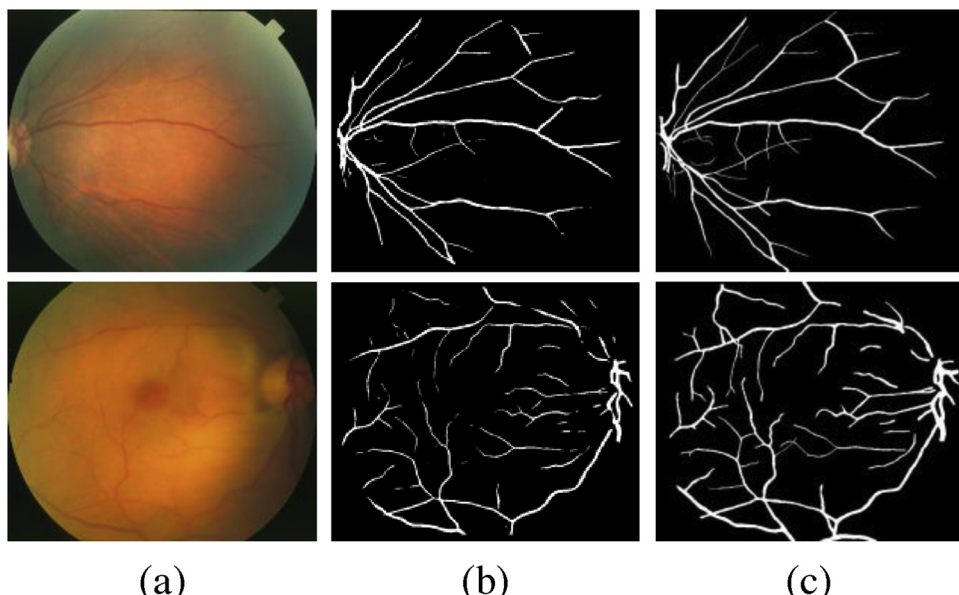


**Fig. 16.** Vessel extraction results for STARE database. (first row) the best case accuracy; (second row) the worst case accuracy. (a) Input image, (b) vessel extraction by proposed method, and (c) 1st Human observer.

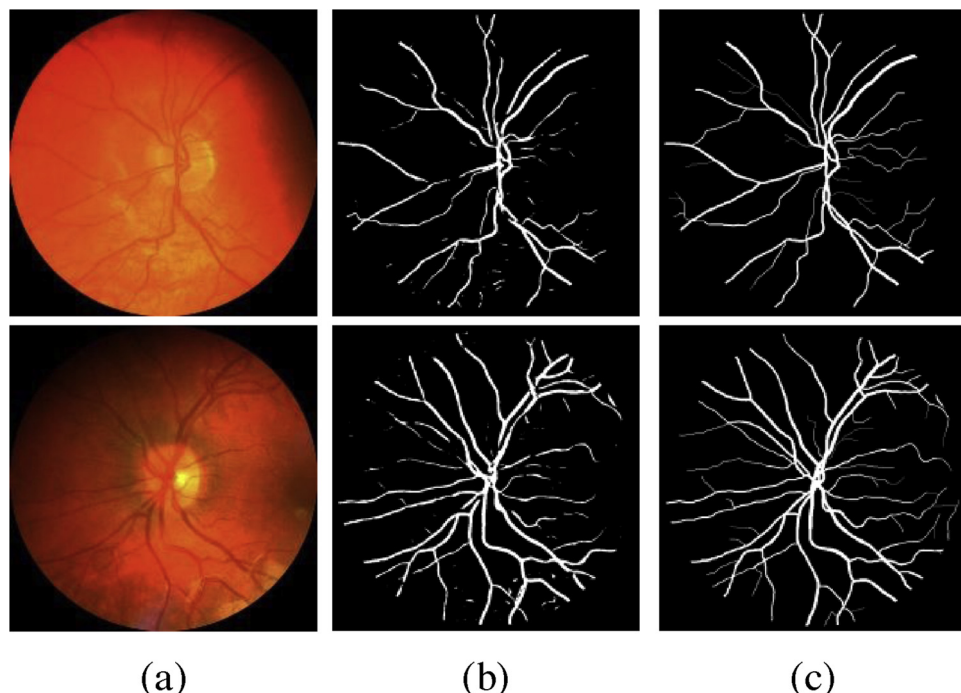


**Fig. 17.** Vessel extraction results for CHASE\_DB1 database. (first row) the best case accuracy; (second row) the worst case accuracy. (a) Input image, (b) vessel extraction by proposed method, and (c) 1st Human observer.

**Table 2**  
Performance measure of cross-training.

| Database  | Method               | Sen    | Spe    | ACC    | AUC    |
|-----------|----------------------|--------|--------|--------|--------|
| DRIVE     | Trained on STARE     | 0.7519 | 0.9807 | 0.9499 | 0.9692 |
|           | Trained on CHASE_DB1 | 0.7560 | 0.9791 | 0.9491 | 0.9623 |
| STARE     | Trained on DRIVE     | 0.7390 | 0.9893 | 0.9630 | 0.9647 |
|           | Trained on CHASE_DB1 | 0.7270 | 0.9875 | 0.9602 | 0.9588 |
| CHASE_DB1 | Trained on STARE     | 0.7429 | 0.9801 | 0.9555 | 0.9599 |
|           | Trained on DRIVE     | 0.7257 | 0.9831 | 0.9564 | 0.9702 |

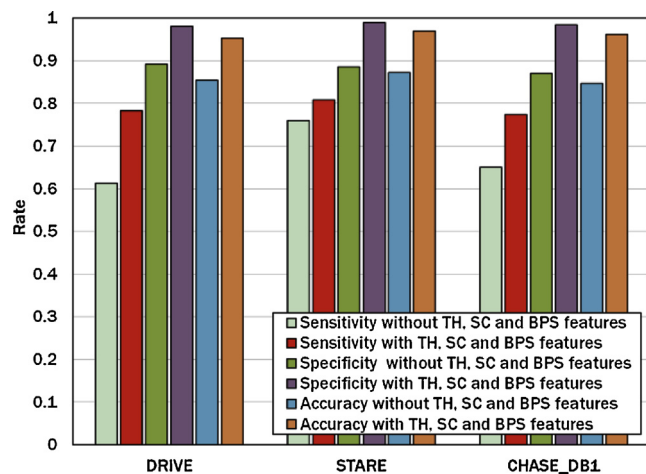


**Fig. 18.** Influence of the utilized features on the system performance.

influence on the improvement of the system performance in terms of the three evaluation criteria on all databases. This shows the informativeness of these features that can help the system to detect the vessels more reliably.

#### 4.6. Experiment 4: influence of the automatic thresholding

Regarding that the quality of the retinal images and the visibility of vessels within them are different in various retinal images, for converting the Gabor images to binary images, we design an automatic thresholding scheme to find a suitable threshold value based on the quality of each image. In order to study the effectiveness of this thresholding method on the system performance, the implemented system is executed once with the common thresholding method proposed by Otsu [67] and once with the proposed automatic thresholding algorithm on three databases. The average results on the whole testing images of each database are shown in Fig. 19. As shown in this figure, the rate of all evaluation metrics are increased when using our thresholding scheme. The improvements on CHASE\_DB1 database are higher than others as it contains images with non-uniform background illumination and poor contrast of blood vessels as compared with the background.

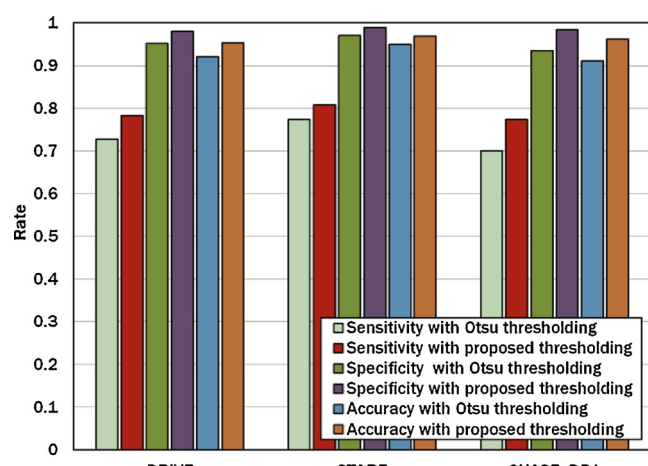


**Fig. 19.** Influence of the automatic thresholding on the system performance.

**Table 3**

Comparison of the proposed method with other methods.

| Method                             | DRIVE         |               |               |               | STARE         |               |               |               | CHASE_DB1     |               |               |               |
|------------------------------------|---------------|---------------|---------------|---------------|---------------|---------------|---------------|---------------|---------------|---------------|---------------|---------------|
|                                    | Sen           | Spe           | ACC           | AUC           | Sen           | Spe           | ACC           | AUC           | Sen           | Spe           | ACC           | AUC           |
| Proposed method                    | 0.7830        | 0.9800        | 0.9531        | 0.9752        | <b>0.8087</b> | <b>0.9892</b> | <b>0.9691</b> | 0.9853        | <b>0.7737</b> | <b>0.9840</b> | <b>0.9623</b> | <b>0.9789</b> |
| Hu, Zhang et al. [12]              | 0.7772        | 0.9793        | 0.9533        | 0.9759        | 0.7543        | 0.9814        | 0.9632        | 0.9751        | —             | —             | —             | —             |
| Aguirre-Ramos et al. [52]          | <b>0.7854</b> | —             | 0.9503        | —             | 0.7116        | 0.9454        | 0.9231        | —             | —             | —             | —             | —             |
| Rodrigues and Marengoni [23]       | 0.7165        | 0.9801        | 0.9465        | —             | —             | —             | —             | —             | —             | —             | —             | —             |
| Zhao, Zhao et al. [48]             | 0.7820        | 0.9790        | <b>0.9570</b> | 0.8860        | 0.7890        | 0.9780        | 0.9560        | 0.8850        | —             | —             | —             | —             |
| Javidi, Pourreza et al. [51]       | 0.7201        | 0.9702        | 0.9450        | —             | 0.7780        | 0.9653        | 0.9517        | —             | —             | —             | —             | —             |
| Li, Feng et al. [5]                | 0.7569        | 0.9716        | 0.9527        | 0.9738        | 0.7726        | 0.9824        | 0.9628        | <b>0.9879</b> | 0.7507        | 0.9793        | 0.9581        | 0.9716        |
| Singh and Srivastava [36]          | 0.7594        | —             | 0.9522        | —             | 0.7939        | —             | 0.9270        | —             | —             | —             | —             | —             |
| Aslani and Sarnel [13]             | 0.7545        | 0.9801        | 0.9513        | 0.9682        | 0.7556        | <b>0.9837</b> | 0.9605        | 0.9789        | —             | —             | —             | —             |
| GeethaRamani et al. [50]*          | 0.7079        | 0.9778        | 0.9536        | —             | —             | —             | —             | —             | —             | —             | —             | —             |
| Vega, Sanchez-Ante et al. [14]     | 0.7444        | 0.9600        | 0.9412        | —             | 0.7019        | 0.9671        | 0.9483        | —             | —             | —             | —             | —             |
| Azzopardi, Strisciuglio et al. [3] | 0.7655        | 0.9704        | 0.9442        | 0.9614        | 0.7716        | 0.9701        | 0.9497        | 0.9563        | 0.7585        | 0.9587        | 0.9387        | 0.9487        |
| Franklin and Rajan [15]            | 0.6867        | <b>0.9824</b> | 0.9503        | —             | —             | —             | —             | —             | —             | —             | —             | —             |
| Saffarzadeh, Osareh et al. [41]    | —             | —             | 0.9387        | 0.9303        | —             | —             | 0.9483        | 0.9431        | —             | —             | —             | —             |
| Akram and Khan [44]                | —             | —             | 0.9469        | 0.9632        | —             | —             | 0.9502        | 0.9706        | —             | —             | —             | —             |
| Fraz, Remagnino et al. [17]        | 0.7406        | 0.9807        | 0.9480        | <b>0.9774</b> | 0.7548        | 0.9763        | 0.9534        | 0.9768        | 0.7224        | 0.9711        | 0.9469        | 0.9712        |
| Fraz, Barman et al. [38]           | 0.7152        | 0.9769        | 0.9430        | —             | 0.7311        | 0.9680        | 0.9442        | —             | —             | —             | —             | —             |
| Miri and Mahloojifar [28]          | 0.7352        | 0.9795        | 0.9458        | —             | —             | —             | —             | —             | —             | —             | —             | —             |
| You, Peng et al. [1]               | 0.7410        | 0.9751        | 0.9434        | —             | 0.7260        | 0.9756        | 0.9497        | —             | —             | —             | —             | —             |
| Lam, Gao et al. [45]               | —             | —             | 0.9472        | 0.9614        | —             | —             | 0.9567        | 0.9739        | —             | —             | —             | —             |
| Zhang, Zhang et al. [35]           | 0.7120        | 0.9724        | 0.9382        | —             | 0.7177        | 0.9753        | 0.9484        | —             | —             | —             | —             | —             |
| Soares, Leandro et al. [18]        | —             | —             | 0.9466        | 0.9614        | —             | —             | 0.9480        | 0.9671        | —             | —             | —             | —             |
| Mendonca and Campilho [37]         | 0.7344        | 0.9764        | 0.9452        | —             | 0.6996        | 0.9730        | 0.9440        | —             | —             | —             | —             | —             |
| Staal, Abramoff et al. [19]        | —             | —             | 0.9442        | 0.9520        | —             | —             | 0.9516        | 0.9614        | —             | —             | —             | —             |

\*Results obtained with a different definition of FOV.

#### 4.7. Experiment 5: comparison with other methods

The performance of the proposed method in terms of the Sen, Spe, Acc and AUC metrics on the DRIVE, STARE and CHASE\_DB1 databases is compared with the state-of-the-art methods. The average performances are provided in Table 3. The performance measures of compared methods are quoted directly from the respective publications. The best rates are bold faced and dashes are used to show that the results are not available (i.e. a method has not used a database in its experiments).

As can be seen from Table 3, the overall performance of the proposed method on all three databases is better than the performance of the other methods. The Acc rates achieved by the proposed method for DRIVE, STARE and CHASE\_DB1 databases are 0.9531, 0.9691 and 0.9623, respectively. These results indicate that, our method outperforms all the methods on STARE and CHASE\_DB1 databases, and only on DRIVE database, it is slightly lower (about 0.0039) than the method proposed in [48]. However, the AUC rate obtained by the proposed method on DRIVE database is much better (about 0.0892) than that of [48]. In addition, although the best Sen, Spe and AUC rates on the DRIVE database belong to the methods proposed in [52,15], and [17], respectively, the overall performance of the proposed method on this database is higher. The Acc rate of the proposed method is about 0.0028 higher than those of [52] and [15]. Also, the Sen and Acc rates of the proposed method are better than those of [17].

It is worth noting that the performance of the method in [50] has been assessed with a different definition of FOV. In this method, the whole image including the surrounding pixels of the FOV has been used for the assessment of the method. So that, its results are not comparable to the other methods which consider only the FOV pixels for evaluation purpose.

For the STARE and CHASE\_DB1 databases, the proposed method outperforms all other methods in terms of the all performance measures, except the method in [5] which its AUC rate just on STARE database is about 0.0026 higher than that of the proposed method. However, the results of the proposed method in terms of all evaluation metrics on the DRIVE and CHASE\_DB1 databases are better than that

method. Also, the Sen, Spe and ACC rates of the proposed method on STARE are higher than that of [5] (0.8087, 0.9892 and 0.9691 versus 0.7726, 0.9824 and 0.9628, respectively).

The average Acc and AUC values obtained by the proposed method on three databases are 0.9615 and 0.9798, respectively. The results confirm that the use of a combination of unsupervised (clustering) and supervised (classification) techniques, and utilizing a set of efficient image features can improve the performance of the retinal blood vessel segmentation task.

#### 5. Conclusion

Retinal blood vessel extraction is usually performed based on two methods: supervised and unsupervised. Till date, various approaches have been presented based on each method, with each having its advantages and shortcomings. In this research, we tried to utilize the advantages of both methods, including the high speed of the unsupervised methods and high accuracy of the supervised methods. Accordingly, a combined approach of two methods was introduced. The proposed method was designed in three phases. The first one was the preprocessing phase that included some image processing steps such as cropping the FOV of the image, color space transformations, and contrast enhancement. The second phase was the vessel extraction process, which started with feature extraction. Further to the common features used in extracting blood vessels, three effective features were utilized in this research: TH, SC and BPS features. The TH feature was used to provide an image with clear vessels. The SC feature was used to improve the system performance against the light intensity variations in the retinal images. The BPS feature was extracted by analyzing the bit planes, which was able to present an image of the orientation map of the blood vessels. Then, the blood vessels were extracted by applying the resultant feature vector of each image pixel in clustering and classification operations. The last phase, i.e. the post-processing step, included a simple masking operation and the output of the finally extracted blood vessels. The proposed method was evaluated on three standard databases: DRIVE, STARE and CHASE\_DB1. By comparing the results of the proposed method with state-of-the-art approaches, it was

confirmed that the proposed method displayed a better performance in retinal blood vessel extraction. Extensive experiments were performed to evaluate the effectiveness of solutions applied in different steps of the proposed method. The results confirmed that each applied technique had a positive influence in improving performance.

As a future direction, it would be of interest to study the effectiveness of any other image features for performance improvement of the proposed method.

## References

- [1] You X, Peng Q, Yuan Y, Y-m Cheung, Lei J. Segmentation of retinal blood vessels using the radial projection and semi-supervised approach. *Pattern Recognit* 2011;44:2314–24.
- [2] Abràmoff MD, Folk JC, Han DP, et al. Automated analysis of retinal images for detection of referable diabetic retinopathy. *JAMA Ophthalmol* 2013;131:351–7.
- [3] Azzopardi G, Strisciuglio N, Vento M, Petkov N. Trainable COSFIRE filters for vessel delineation with application to retinal images. *Med Image Anal* 2015;19:46–57.
- [4] Kirbas C, Quek F. A review of vessel extraction techniques and algorithms. *ACM Comput Surv* 2004;36:81–121.
- [5] Li Q, Feng B, Xie L, Liang P, Zhang H, Wang T. A cross-modality learning approach for vessel segmentation in retinal images. *IEEE Trans Med Imaging* 2016;35:109–18.
- [6] Marin D, Aquino A, Gegundez-Arias ME, Bravo JM. A new supervised method for blood vessel segmentation in retinal images by using gray-level and moment invariants-based features. *IEEE Trans Med Imaging* 2011;30:146–58.
- [7] Mo J, Zhang L. Multi-level deep supervised networks for retinal vessel segmentation. *Int J Comput Assist Radiol Surg* 2017;12:2181–93.
- [8] Zhu C, Zou B, Zhao R, Cui J, Duan X, Chen Z, et al. Retinal vessel segmentation in colour fundus images using Extreme Learning Machine. *Comput Med Imaging Graph* 2017;55:68–77.
- [9] Akbar S, Akram MU, Sharif M, Tariq A, Khan SA. Decision support system for detection of hypertensive retinopathy using arteriovenous ratio. *Artif Intell Med* 2018.
- [10] Saleh E, Blaszczyński J, Moreno A, Valls A, Romero-Aroca P, de la Riva-Fernández S, et al. Learning ensemble classifiers for diabetic retinopathy assessment. *Artif Intell Med* 2018;85:50–63.
- [11] Pereira C, Veiga D, Mahdjoub J, Guessoum Z, Gonçalves I, Ferreira M, et al. Using a multi-agent system approach for microaneurysm detection in fundus images. *Artif Intell Med* 2014;60:179–88.
- [12] Hu K, Zhang Z, Niu X, Zhang Y, Cao C, Xiao F, et al. Retinal vessel segmentation of color fundus images using multiscale convolutional neural network with an improved cross-entropy loss function. *Neurocomputing* 2018;309:179–91.
- [13] Aslani S, Sarnel H. A new supervised retinal vessel segmentation method based on robust hybrid features. *Biomed Signal Process Control* 2016;30:1–12.
- [14] Vega R, Sanchez-Ante G, Falcon-Morales LE, Sossa H, Guevara E. Retinal vessel extraction using Lattice Neural Networks with dendritic processing. *Comput Biol Med* 2015;58:20–30.
- [15] Franklin SW, Rajan SE. Computerized screening of diabetic retinopathy employing blood vessel segmentation in retinal images. *Biocybern Biomed Eng* 2014;34:117–24.
- [16] Fraz MM, Remagnino P, Hoppe A, Barman SA. Retinal image analysis aimed at extraction of vascular structure using linear discriminant classifier. 2013 International Conference on Computer Medical Applications (ICCPMA). 2013. p. 1–6.
- [17] Fraz MM, Remagnino P, Hoppe A, Uyyanonvara B, Rudnicka AR, Owen CG, et al. An ensemble classification-based approach applied to retinal blood vessel segmentation. *IEEE Trans Biomed Eng* 2012;59:2538–48.
- [18] Soares JVB, Leandro JJJ, Cesar RM, Jelinek HF, Cree MJ. Retinal vessel segmentation using the 2-D Gabor wavelet and supervised classification. *IEEE Trans Med Imaging* 2006;25:1214–22.
- [19] Staal J, Abramoff MD, Niemeijer M, Viergever MA, Ginneken Bv. Ridge-based vessel segmentation in color images of the retina. *IEEE Trans Med Imaging* 2004;23:501–9.
- [20] Annunziata R, Garzelli A, Ballerini L, Mecocci A, Trucco E. Leveraging multiscale hessian-based enhancement with a novel exudate inpainting technique for retinal vessel segmentation. *IEEE J Biomed Health Inform* 2016;20:1129–38.
- [21] Frucci M, Riccio D, Sanniti di Baja G, Serino L. Severe: segmenting vessels in retina images. *Pattern Recognit Lett* 2016;82:162–9.
- [22] Savelli B, Marchesi A, Bria A, Marrocco C, Molinara M, Tortorella F. Retinal vessel segmentation through denoising and mathematical morphology. In: Battiatto S, Gallo G, Schettini R, Stanco F, editors. *Image Analysis and Processing - ICIAP 2017: 19th International Conference* 2017:267–76.
- [23] Rodrigues LC, Marengoni M. Segmentation of optic disc and blood vessels in retinal images using wavelets, mathematical morphology and Hessian-based multi-scale filtering. *Biomed Signal Process Control* 2017;36:39–49.
- [24] Challoob M, Gao Y. Retinal vessel segmentation using matched filter with joint relative entropy. In: Felsberg M, Heyden A, Krüger N, editors. *Computer Analysis of Images and Patterns: 17th International Conference, CAIP 2017* 2017:228–39.
- [25] Kumar D, Pramanik A, Kar SS, Maity SP. Retinal blood vessel segmentation using matched filter and Laplacian of Gaussian. 2016 International Conference on Signal Processing and Communications (SPCOM). 2016. p. 1–5.
- [26] Malek J, Azar AT, Nasralla B, Tekari M, Kamoun H, Tourki R. Computational analysis of blood flow in the retinal arteries and veins using fundus image. *Comput Math Appl* 2015;69:101–16.
- [27] Hassan G, El-Bendary N, Hassanean AE, Fahmy A, Abullah MS, Snasel V. Retinal blood vessel segmentation approach based on mathematical morphology. *Procedia Comput Sci* 2015;65:612–22.
- [28] Miri MS, Mahloojifar A. Retinal image analysis using curvelet transform and multistructure elements morphology by reconstruction. *IEEE Trans Biomed Eng* 2011;58:1183–92.
- [29] Sum KW, Cheung PYS. Vessel extraction under non-uniform illumination: a level set approach. *IEEE Trans Biomed Eng* 2008;55:358–60.
- [30] Fraz MM, Remagnino P, Hoppe A, Uyyanonvara B, Rudnicka AR, Owen CG, et al. Blood vessel segmentation methodologies in retinal images – a survey. *Comput Methods Programs Biomed* 2012;108:407–33.
- [31] Wang S, Yin Y, Cao G, Wei B, Zheng Y, Yang G. Hierarchical retinal blood vessel segmentation based on feature and ensemble learning. *Neurocomputing* 2015;149:708–17.
- [32] Ricci E, Perfetti R. Retinal blood vessel segmentation using line operators and support vector classification. *IEEE Trans Med Imaging* 2007;26:1357–65.
- [33] Bezdek JC, Ehrlich R, Full W. FCM: the fuzzy c-means clustering algorithm. *Comput Geosci* 1984;10:191–203.
- [34] Hoover A, Kouzenetsova V, Goldbaum M. Locating blood vessels in retinal images by piecewise threshold probing of a matched filter response. *IEEE Trans Med Imaging* 2000;19:203–10.
- [35] Zhang B, Zhang L, Zhang L, Karayannidis F. Retinal vessel extraction by matched filter with first-order derivative of Gaussian. *Comput Biol Med* 2010;40:438–45.
- [36] Singh NP, Srivastava R. Retinal blood vessels segmentation by using Gumbel probability distribution function based matched filter. *Comput Methods Programs Biomed* 2016;129:40–50.
- [37] Mendonça AM, Campilho A. Segmentation of retinal blood vessels by combining the detection of centerlines and morphological reconstruction. *IEEE Trans Med Imaging* 2006;25:1200–13.
- [38] Fraz MM, Barman SA, Remagnino P, Hoppe A, Basit A, Uyyanonvara B, et al. An approach to localize the retinal blood vessels using bit planes and centerline detection. *Comput Methods Programs Biomed* 2012;108:600–16.
- [39] Quck FKH, Kirbas C. Vessel extraction in medical images by wave-propagation and traceback. *IEEE Trans Med Imaging* 2001;20:117–31.
- [40] Wink O, Niessen WJ, Viergever MA. Multiscale vessel tracking. *IEEE Trans Med Imaging* 2004;23:130–3.
- [41] Saffarzadeh VM, Osareh A, Shadgar B. Vessel segmentation in retinal images using multi-scale line operator and K-Means clustering. *J Med Signals Sens* 2014;4:122–9.
- [42] Hou Y. Automatic segmentation of retinal blood vessels based on improved multi-scale line detection. *J Comput Sci Eng* 2014;8:119–28.
- [43] Anzalone A, Bizzarri F, Parodi M, Storace M. A modular supervised algorithm for vessel segmentation in red-free retinal images. *Comput Biol Med* 2008;38:913–22.
- [44] Akram MU, Khan SA. Multilayered thresholding-based blood vessel segmentation for screening of diabetic retinopathy. *Eng Comput* 2013;29:165–73.
- [45] Lam BSY, Gao Y, Liew AWC. General retinal vessel segmentation using regularization-based multicavity modeling. *IEEE Trans Med Imaging* 2010;29:1369–81.
- [46] Chan TF, Vese LA. Active contours without edges. *IEEE Trans Image Process* 2001;10:266–77.
- [47] Al-Diri B, Hunter A, Steel D. An active contour model for segmenting and measuring retinal vessels. *IEEE Trans Med Imaging* 2009;28:1488–97.
- [48] Zhao Y, Zhao J, Yang J, Liu Y, Zhao Y, Zheng Y, et al. Saliency driven vasculature segmentation with infinite perimeter active contour model. *Neurocomputing* 2017;259:201–9.
- [49] Niemeijer M, Staal J, van Ginneken B, Loog M, Abramoff MD. Comparative study of retinal vessel segmentation methods on a new publicly available database. *SPIE medical imaging: SPIE*; 2004. p. 648–56.
- [50] GeethaRamani R, Balasubramanian L. Retinal blood vessel segmentation employing image processing and data mining techniques for computerized retinal image analysis. *Biocybern Biomed Eng* 2016;36:102–18.
- [51] Javidi M, Pourreza H-R, Harati A. Vessel segmentation and microaneurysm detection using discriminative dictionary learning and sparse representation. *Comput Methods Programs Biomed* 2017;139:93–108.
- [52] Aguirre-Ramos H, Avina-Cervantes JG, Cruz-Aceves I, Ruiz-Pinales J, Ledesma S. Blood vessel segmentation in retinal fundus images using Gabor filters, fractional derivatives, and Expectation Maximization. *Appl Math Comput* 2018;339:568–87.
- [53] Bhuiyan A, Nath B, Chua J, Ramamohanarao K. Automatic detection of vascular bifurcations and crossovers from color retinal fundus images. 2007 Third International IEEE Conference on Signal-Image Technologies and Internet-Based System. 2007. p. 711–8.
- [54] Reza AM. Realization of the contrast limited adaptive histogram equalization (CLAHE) for real-time image enhancement. *J VLSI Signal Process Syst Signal Image Video Technol* 2004;38:35–44.
- [55] Pizer SM, Amburn EP, Austin JD, Cromartie R, Geselowitz A, Greer T, et al. Adaptive histogram equalization and its variations. *Comput Vis Graph Image Process* 1987;39:355–68.
- [56] Fogel I, Sagi D. Gabor filters as texture discriminator. *Biol Cybern* 1989;61:103–13.
- [57] Ramligum GS, Nagarajan VK, Chakraborty C. Small retinal vessels extraction towards proliferative diabetic retinopathy screening. *Expert Syst Appl* 2012;39:1141–6.
- [58] Qin L, Lei Z, Zhang D, Bhattacharya P. A new approach to automated retinal vessel segmentation using multiscale texture. 18th International Conference on Pattern Recognition (ICPR'06). 2006. p. 77–80.
- [59] Fraz MM, Remagnino P, Hoppe A, Velastin S, Uyyanonvara B, Barman SA. A supervised method for retinal blood vessel segmentation using line strength, multi-scale gabor and morphological features. 2011 IEEE International Conference on Signal and Image Processing Applications (ICSIPA). 2011. p. 410–5.

- [60] Bhuiyan A, Nath B, Chua J, Kotagiri R. Blood vessel segmentation from color retinal images using unsupervised texture classification. 2007 IEEE International Conference on Image Processing. 2007. p. V - 521-V - 4.
- [61] van Vliet LJ, Young IT, Beckers GL. A nonlinear laplace operator as edge detector in noisy images. *Comput Vis Graph Image Process* 1989;45:167–95.
- [62] Kittler J, Illingworth J. Minimum error thresholding. *Pattern Recognit* 1986;19:41–7.
- [63] Niemeijer M, Bv Ginneken, Staal J, Suttorp-Schulten MSA, Abramoff MD. Automatic detection of red lesions in digital color fundus photographs. *IEEE Trans Med Imaging* 2005;24:584–92.
- [64] Wold S, Esbensen K, Geladi P. Principal component analysis. *Chemom Intell Lab Syst* 1987;2:37–52.
- [65] Jolliffe IT. Principal component analysis and factor analysis. *Principal component analysis*. New York, NY: Springer New York; 1986. p. 115–28.
- [66] Ramani RG, Balasubramanian L, Meenal A. A hybrid classification model employing Genetic algorithm and Root guided Decision Tree for improved categorization of data. *ARPN J Eng Appl Sci* 2015;10:9968–75.
- [67] Otsu N. A threshold selection method from gray-level histograms. *IEEE Trans Syst Man Cybern* 1979;9:62–6.